High-Lift Systems

Outline of this Chapter

The chapter is divided into four sections. The introduction describes the motivation for high lift systems, and the basic concepts underlying flap and slat systems. The second section deals with the basic ideas behind high lift performance prediction, and the third section details the specific method used here for estimating C_{Lmax}. Some discussion on maximum lift prediction for supersonic aircraft concludes the chapter.

High Lift Systems -- Introduction

A wing designed for efficient high-speed flight is often quite different from one designed solely for take-off and landing. Take-off and landing distances are strongly influenced by aircraft stalling speed, with lower stall speeds requiring lower acceleration or deceleration and correspondingly shorter field lengths. It is always possible to reduce stall speed by increasing wing area, but it is not desirable to cruise with hundreds of square feet of extra wing area (and the associated weight and drag), area that is only needed for a few minutes. Since the stalling speed is related to wing parameters by:

$$V_{stall} = (2W/(S\rho C_{Lmax}))^{1/2}$$

It is also possible to reduce stalling speed by reducing weight, increasing air density, or increasing wing C_{Lmax} . The latter parameter is the most interesting. One can design a wing airfoil that compromises cruise efficiency to obtain a good C_{Lmax} , but it is usually more efficient to include movable leading and/or trailing edges so that one may obtain good high speed performance while achieving a high C_{Lmax} at take-off and landing. The primary goal of a high lift system is a high C_{Lmax}; however, it may also be desirable to maintain low drag at take-off, or high drag on approach. It is also necessary to do this with a system that has low weight and high reliability.

This is generally achieved by incorporating some form of trailing edge flap and perhaps a leading edge device such as a slat.

Flap Geometry

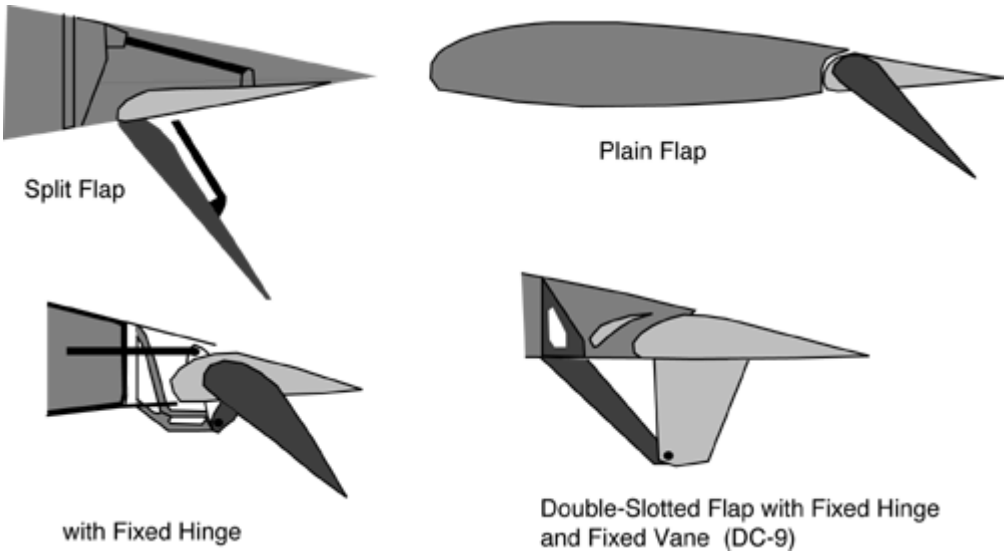

Figure 1. Flap System Geometries

Figure 2. The triple-slotted flap system used on a 737.

Figure 3 shows a double-slotted flap and slat system (a 4-element airfoil). Here, some of the increase in C_{Lmax} is associated with an increase in chord length (Fowler motion) provided by motion along the flap track or by a rotation axis that is located below the wing.

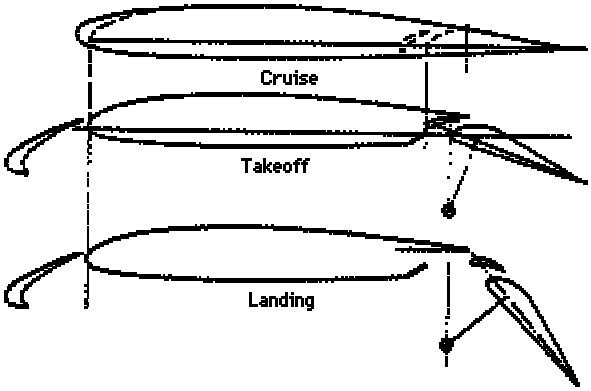

Figure 3. Double-Slotted Flap and Slat System

Modern high lift systems are often quite complex with many elements and multi-bar linkages. Here is a double-slotted flap system as used on a DC-8. For some time Douglas resisted the temptation to use tracks and resorted to such elaborate 4-bar linkages. The idea was that these would be more reliable. In practice, it seems both schemes are very reliable. Current practice has been to simplify the flap system and double (or even single) slotted systems are often preferred.

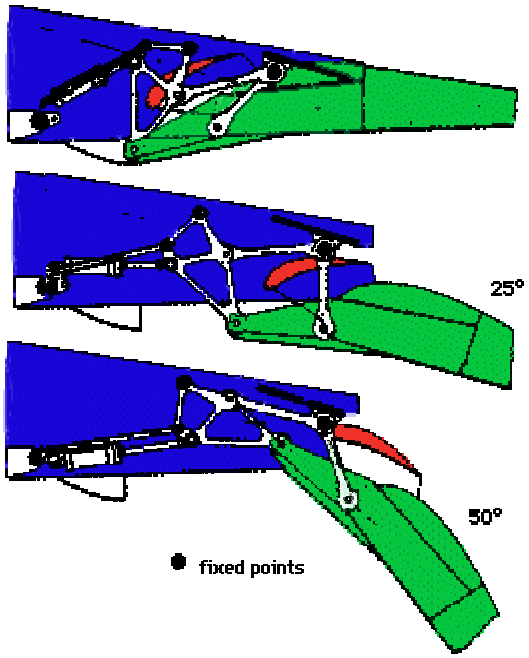

Figure 4. Motion of a Double-Slotted Flap

Flap Aerodynamics

Flaps change the airfoil pressure distribution, increasing the camber of the airfoil and allowing more of the lift to be carried over the rear portion of the section. If the maximum lift coefficient is controlled by the height of the forward suction peak, the flap permits more lift for a given peak height. Flaps also increase the lift at a given angle of attack, important for aircraft which are constrained by ground angle limits. Typical results are shown in figure 5 from data on a DC-9-30, a configuration very similar to the Boeing 717.

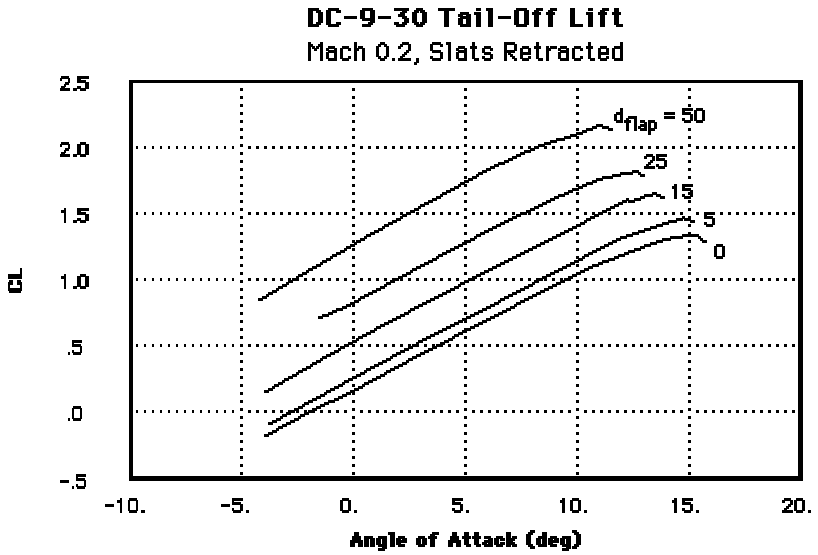

Figure 5. DC-9-30 CL vs. Flap Deflection and Angle-of-Attack

Slotted flaps achieve higher lift coefficients than plain or split flaps because the boundary layer that forms over the flap starts at the flap leading edge and is "healthier" than it would have been if it had

traversed the entire forward part of the airfoil before reaching the flap. The forward segment also achieves a higher C_{lmax} than it would without the flap because the pressure at the trailing edge is reduced due to interference, and this reduces the adverse pressure gradient in this region.

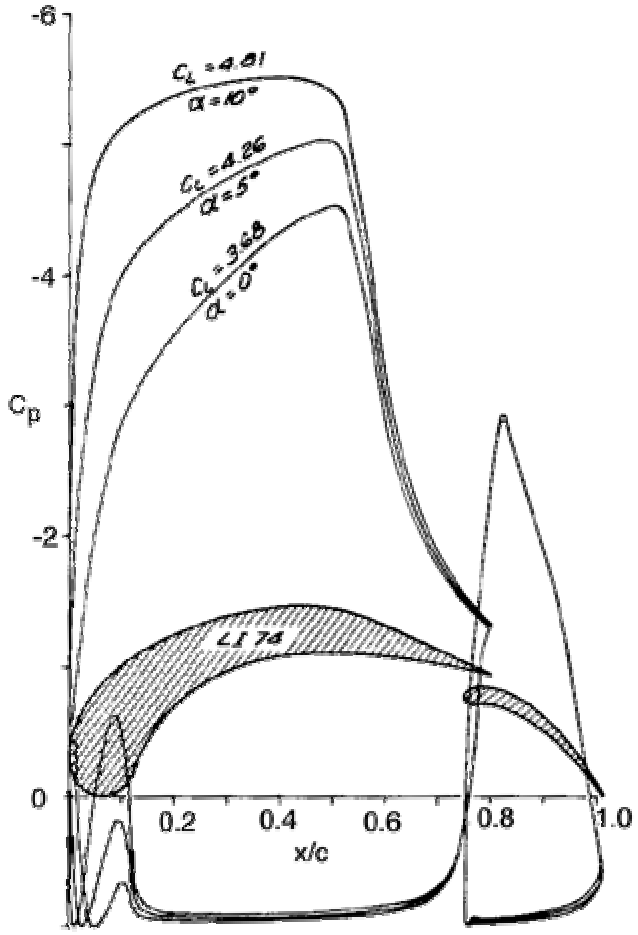

Figure 6. Maximum Lift Slotted Section.

The favorable effects of a slotted flap on C_{lmax} was known early in the development on high lift systems. That a 2-slotted flap is better than a single-slotted flap and that a triple-slotted flap achieved even higher C_l's suggests that one might try more slots. Handley Page did this in the 1920's. Tests showed a C_{lmax} of almost 4.0 for a 6-slotted airfoil.

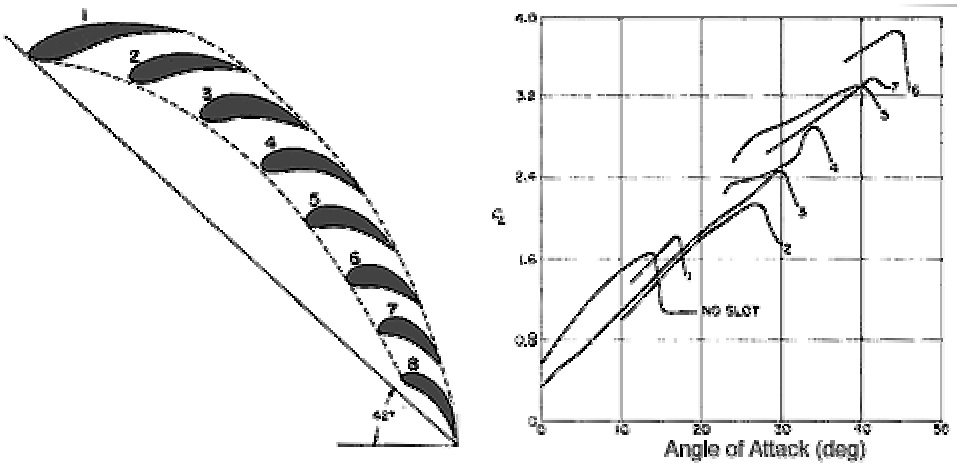

Figure 7. Results for a multi-element section from 1921.

Leading Edge Devices

Leading edge devices such as nose flaps, Kruger flaps, and slats reduce the pressure peak near the nose by changing the nose camber. Slots and slats permit a new boundary layer to start on the main wing portion, eliminating the detrimental effect of the initial adverse gradient.

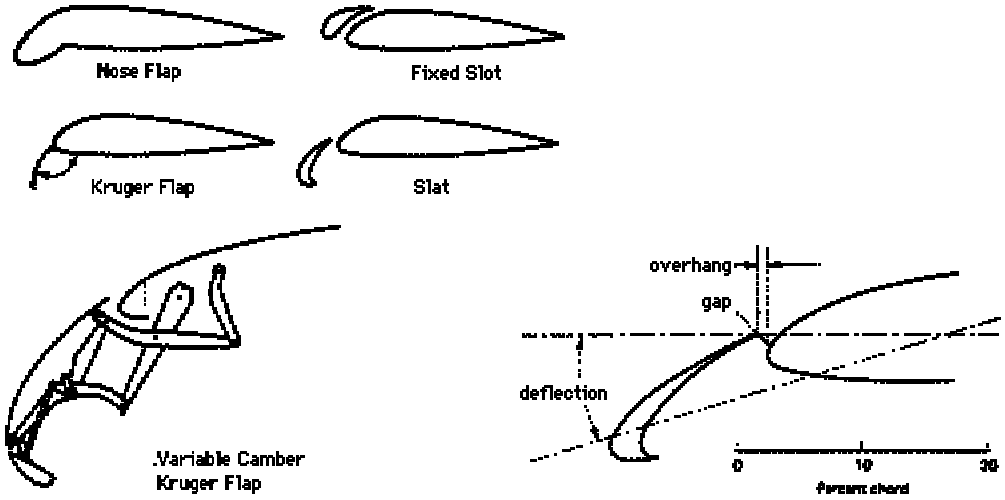

Figure 8. Leading Edge Devices

Slats operate rather differently from flaps in that they have little effect on the lift at a given angle of attack. Rather, they extend the range of angles over which the flow remains attached. This is shown in figure 9.

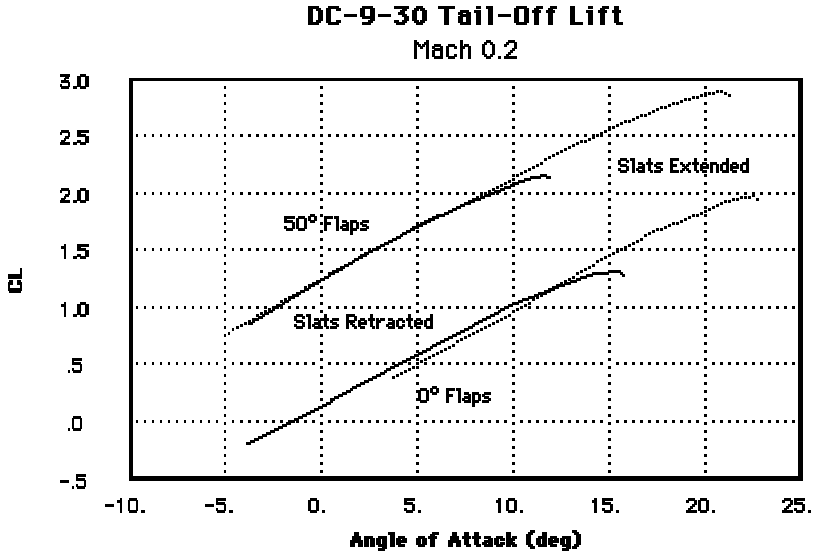

Figure 9. Effect of Slats on Lift Curve. Dotted curves are slats extended; solid curves show slats retracted.

Today computational fluid dynamics is used to design these complex systems; however, the prediction of C_{Lmax} by direct computation is still difficult and unreliable. Wind tunnel tests are also

difficult to interpret due to the sensitivity of C_{Lmax} to Reynolds number and even freestream turbulence levels.

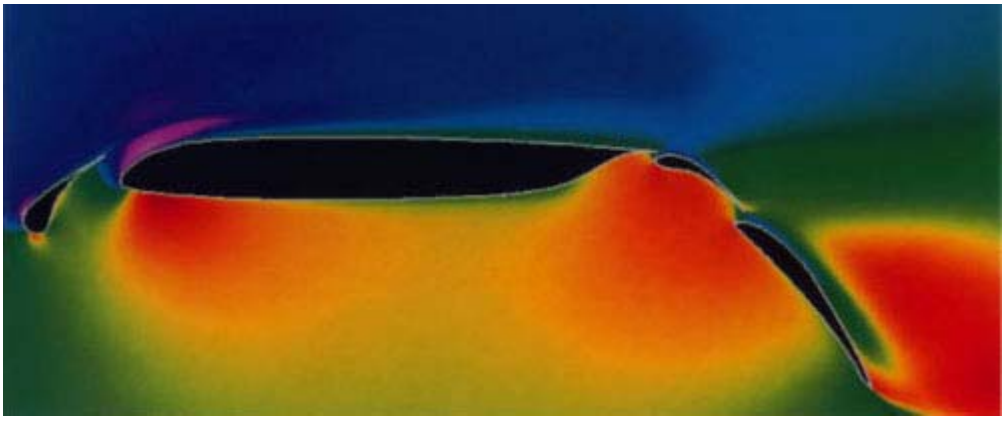

Figure 10. Navier-Stokes computations of the flow over a 4-element airfoil section (NASA)

Maximum Lift Prediction -- General Approach

The calculation of C_{Lmax} is difficult because we must deal with a flow that is viscous, compressible, and highly three-dimensional. Generally, one does not use a Navier-Stokes calculation to estimate maximum lift. This is partly because it takes a very long time to generate a grid and then solve the equations. However, it is also is difficult to estimate the effects of stall strips, fences, and vortex generators that are routinely used on wings and are essential to obtaining acceptable stalling characteristics. Thus, the more usual approach is as follows. The distribution of pressure on the wing is computed from a 3-D panel method. The pressure distributions along streamwise strips are used as input to a two-dimensional boundary layer calculation in which the onset of separation is predicted. The actual maximum lift coefficient is based on the boundary layer data, sometimes supplemented with 2-D wind tunnel data.

In the absence of even 2D boundary layer computations, a variety of simpler rules are used. One of these, the pressure difference rule, has been applied frequently to aircraft with high lift systems. Experiments show that the difference between the peak C_p and the C_p at the trailing edge at C_{lmax} varies with Mach number and Reynolds number. This has been correlated in a number of proprietary rules, but for turbulent sections at low Mach number, it varies roughly from 7 or 8 at a Reynolds number of 1 million to as much at 13 or 14 at 6 million and above. Viscous corrections are made to the results of an inviscid panel method (including a reduction in effective flap deflection due to boundary layer decambering) and then the pressure difference rule applied to each section along the span.

This method usually works well, but many approximations are made. The process of high lift prediction therefore relies strongly on wind tunnel data. But, since the flow is sensitive to changes in

Reynolds number, good 3-D measurements are rare. This is often one of the areas of greatest uncertainty in aircraft design.

At the early stages of design, it is not possible to run even a panel code and 2-D boundary layer analysis. In such cases, one may compute the distribution of wing lift with a vortex lattice method or Weissinger model and compare the distribution of section C_l with the C_{lmax}, estimated from 2-D data. One provides some margin against stalling of the outer panels to account for aileron deflections and spanwise boundary layer flow. When flaps are deflected, sections just outboard of the flap tend to stall early according to this method. In reality, the flow near the flap edge induces effective camber in the adjacent sections and so their maximum lift coefficient is increased. This effect must be included if reliable estimates of C_{Lmax} are to be obtained using this "critical section" approach.

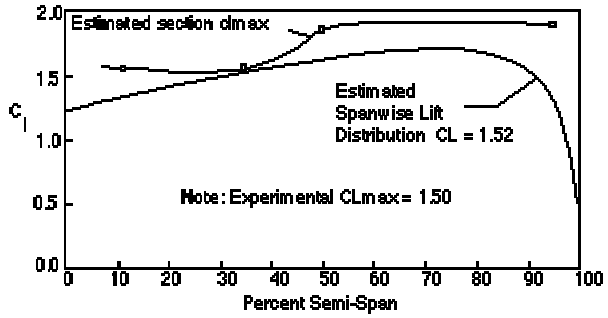

Figure 1. Critical Section Method for C_{Lmax} Prediction: Compute C_L at which most critical 2D section reaches C_{lmax}.

One might be concerned that the use of 2-D maximum lift data is completely inappropriate for computation of wing C_{Lmax} because of 3-D viscous effects. This issue was investigated by NACA in Report 1339. A figure from this paper is reproduced below (Figure 2). It indicates that the "clean wing" C_{Lmax} is, in fact, rather poorly predicted by the critical section method. However, when wing fences are used to prevent spanwise boundary layer flow, the C_{lmax} is increased dramatically and does follow the 2-D results quite well over the outer wing sections. The inboard C_{lmax} is considerably higher than would be expected by strip theory, but inboard section C_{lmax} values are generally reduced with the use of stall strips or other devices to make them stall before the tips. Thus, the tip C_{lmax} and lift distribution determine what the inboard C_{lmax} must be to obtain good stall behavior.

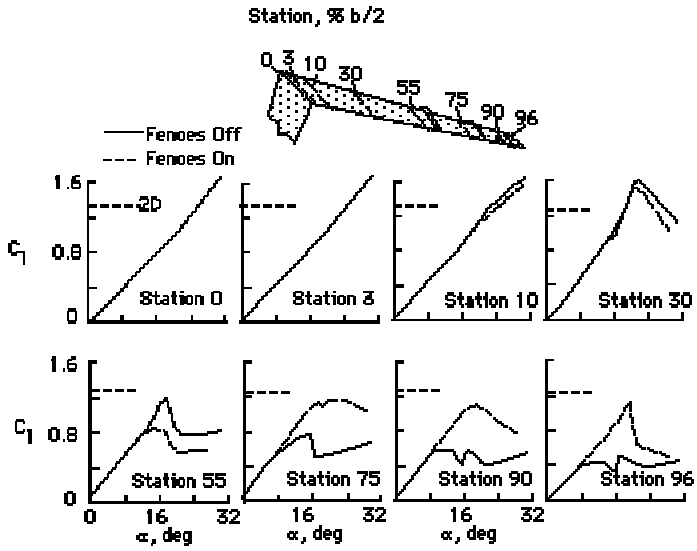

Figure 2. Effect of fences on the section lift coefficients of a sweptback wing. Λ = 45° AR = 8.0, taper = .45, NACA 63(1)A-012 section. Data from NACA Rpt. 1339 Note the result that with fences, outer panel section C_l's are nearly their 2-D values.

Maximum Lift Prediction -- Specific Conceptual Design Method

When the distribution of lift is not computed, it is still possible to make a rough estimate of maximum lift capability. This section describes a simple method appropriate for early design of conventional aircraft.

Outer Panel Section C_{lmax}

One starts by estimating the section C_{lmax} of the outer wing panels. If the airfoil is known, this value may be based on experimental data or computations. A typical variation of section C_{lmax} with thickness for peaky-type transport aircraft airfoils is shown in figure 1. Note that outer panel airfoil thickness ratio is generally less than the average value. Assuming that the outer panel has a t/c about 90% of the average value is reasonable. The increase in C_{lmax} with thickness up to about 12%-15% reflects the larger nose radius of the thicker airfoils. Increased nose radius reduces the leading edge suction peak, the associated adverse pressure gradient, and the tendency to stall. Since supercritical airfoils have large nose radii, their C_{lmax} is about 0.1 greater than the conventional sections shown here.

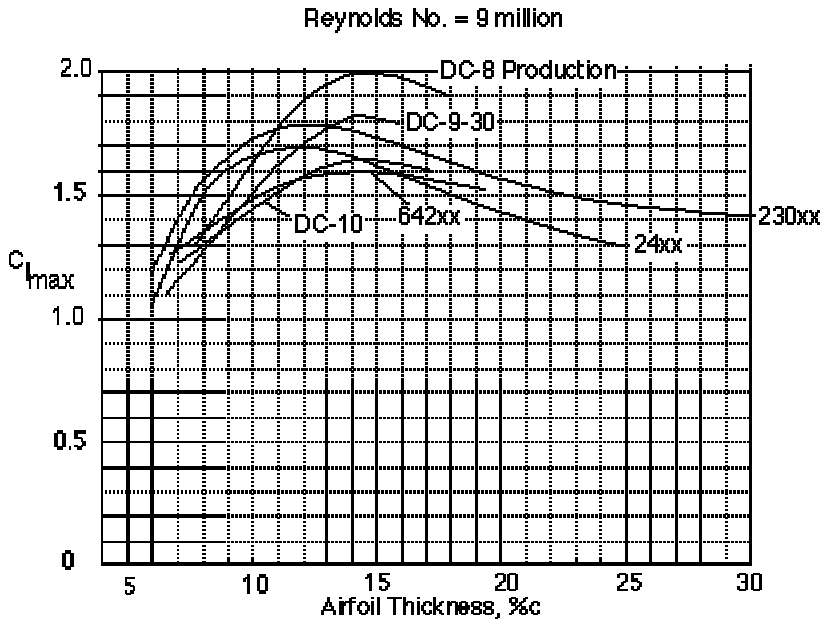

Figure 1. Section C_{lmax} for Various Families of Airfoils.

The section C_{lmax} is also affected by Reynolds number. Some data on this effect is shown in figure 2. The effect of Reynolds number is sometimes very difficult to predict as it changes the location of laminar transition and boundary layer thickness. Thin airfoils are less Reynolds number sensitive, thick sections are more sensitive and show effects up to 15 million.

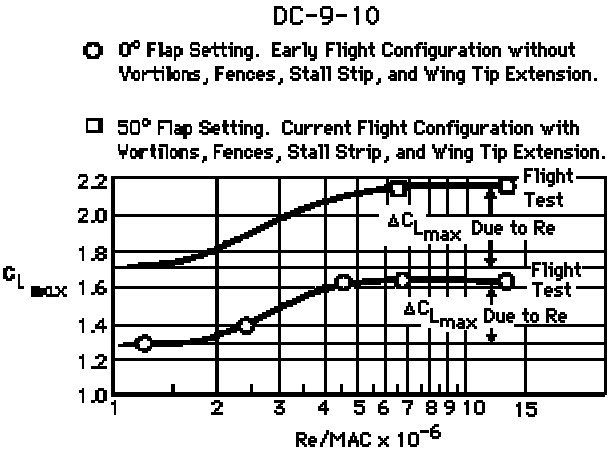

Figure 2. Effect of Reynolds Number

Recent experiments have suggested that, especially for slotted flap systems, significant variations with Reynolds number may occur even above Reynolds numbers of 6 to 9 million. But for initial design purposes, the variation of C_{lmax} with Reynolds number may be approximated by:

$C_{lmax} = C_{lmax\_ref} * (Re / Re_{ref})^{0.1}$

Relating Wing C_{Lmax} to Outer Panel C_{lmax}

The plot in figure 3 shows the ratio of wing C_{Lmax} to the section C_{lmax} of the outer wing panel as a function of wing sweep angle and taper ratio. This plot was constructed by computing the span load distribution of wings with typical taper ratios and twist distributions. The results include a reduction in C_{Lmax} due to tail download of about 0.05, a value typical of conventional aircraft; they also include a suitable margin against outer panel stall. (This margin is typically about 0.2 in C_l.) When estimating the C_{lmax} of the wing outer panel, one should use the chord of the outer panel (typ. at about 75% semi-span) to compute the Reynolds number effect on that section.

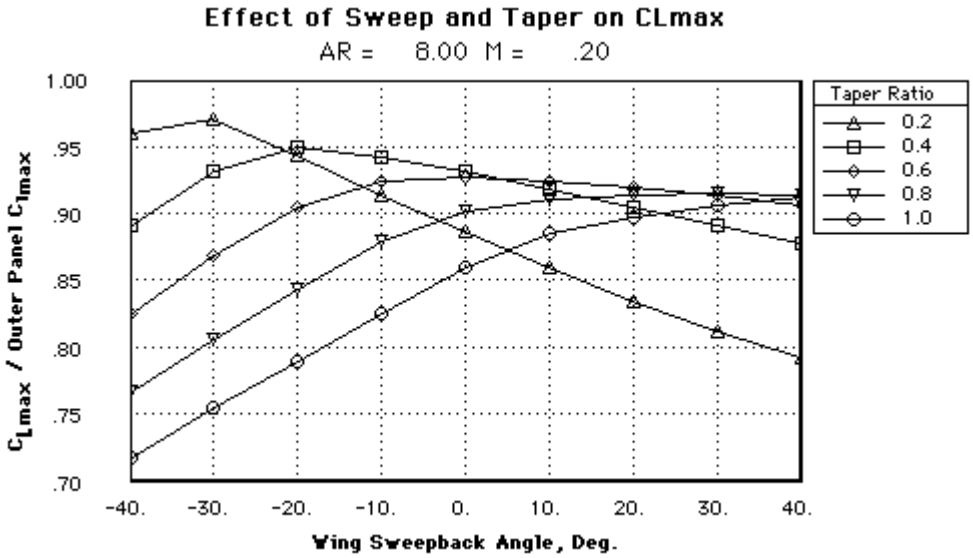

Figure 3. Effect of Taper and Sweep on Wing / Outer Panel C_{lmax}

Additional corrections to wing C_{Lmax}

FAR Stall Speed

The formula for stalling speed given earlier in this section refers to the speed at which the airplane stalls in unaccelerated (1-g) flight. However, for the purposes of certificating a transport aircraft, the Federal Aviation Agency defines the stalling speed as the minimum airspeed flyable at a rate of approach to the stall of one knot per second. Slower speeds than that corresponding to 1-g maximum lift may be demonstrated since no account is taken of the normal acceleration. The maximum lift coefficient calculated from the FAA stall speed is referred to as the minimum speed C_{Lmax} or C_{Lmax_Vmin}. The increment above the 1-g C_{Lmax} is a function of the shape of the lift, drag, and moment curves beyond the stall. These data are not usually available for a new design but examination of available flight test data indicate that C_{Lmax_Vmin}averages about 11% above the 1-g value (based on models DC-7C, DC-8, and KC-135). A typical time history of the dynamic stall maneuver is shown in figure 4.

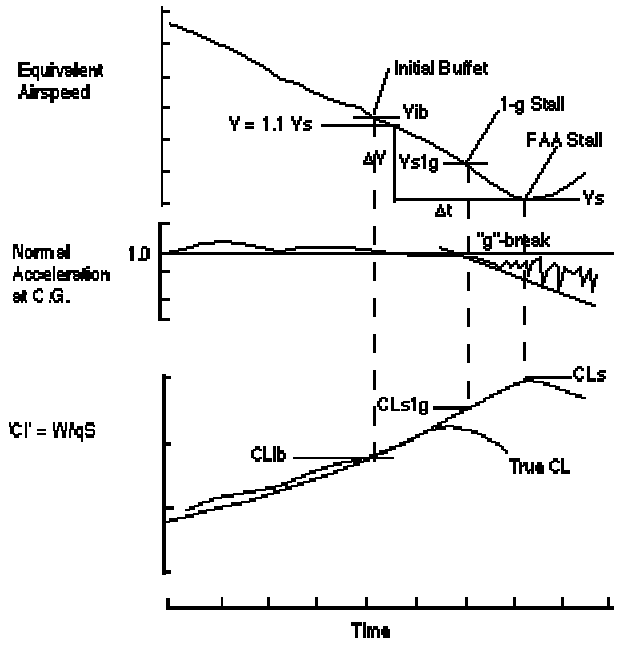

Figure 4. Typical Record of Dynamic Stall Maneuver Power-off Stall, Thrust Effect Negligible, Trim Speed 1.3 to 1.4 V_s, Wings Held Level, Speed Controlled by Elevator

FAR Stall C_L is value of C_{Ls} when DV/Dt = 1kt/sec and: $C_{Ls} = 2W / S\ r\ V_s^2$

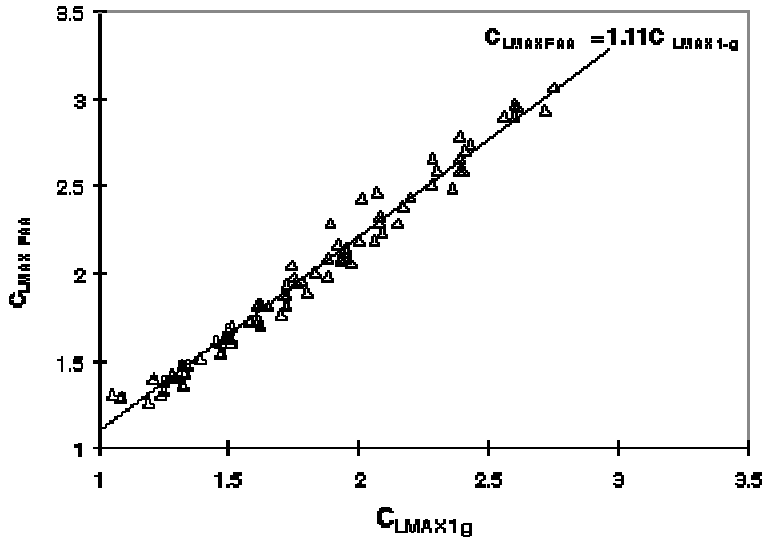

Figure 5. Flight Data showing FAA C_{Lmax} vs. C_{Lmax} based on 1-g flight.

Wing-Mounted Engines

The presence of engine pylons on the wings reduces C_{Lmax}. On the original DC-8 design, the reduction associated with pylons was 0.2. When the pylons are "cut-back" so they do not extend over the top of the leading edge, the reduction can be kept to within about 0.1 with respect to the best clean-wing value.

Increment in C_{Lmax} Due to Slats

When leading edge slats are deployed, the leading edge pressure peak is suppressed. The

introduction of a gap between the leading edge device and the wing leading edge increases the energy of boundary layer above what it would have been without a gap. For this reason, the section lift coefficient is increased dramatically. The specific amount depends on the detailed design of the slat, its deflection, and the gap size. For the purposes of our preliminary design work, the value is estimated based on Douglas designs shown in figure 6. The effect of sweep reduces the lift increment due to slats by the factor shown in figure 7. A better method would include the observation that when leading edge devices are employed, the favorable effect of nose radius (and increased t/c) would not be realized. Although this data applies for 5 deg of flap deflection, this slat increment can be used for preliminary estimates at all flap angles.

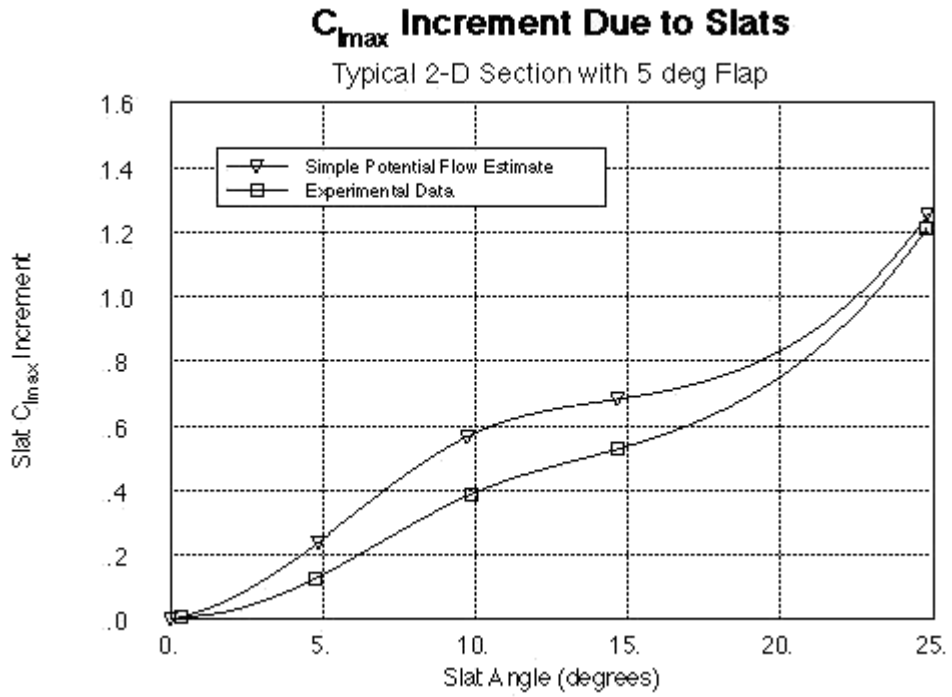

Figure 6. Effect of slat deflection on C_{lmax} increment due to slats. Prediction based on maximum Mach number constraint. This data is for a 17% slat.

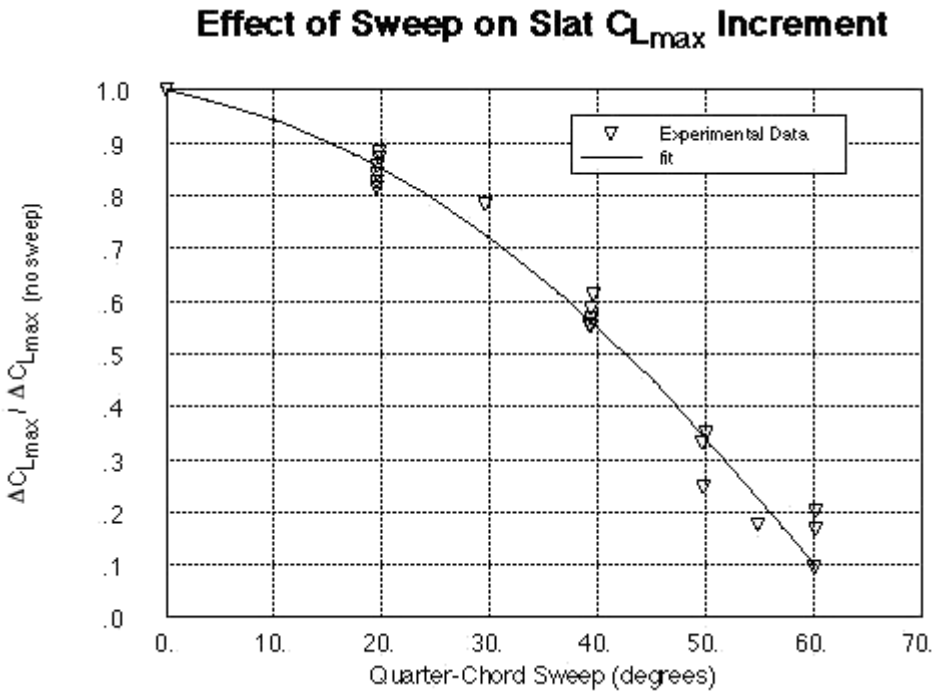

Figure 7. Effect of wing sweep on slat maximum lift increment.

Increment in C_{Lmax} Due to Flaps

A simple method for estimating the C_{Lmax} increment for flaps is described by the following expression. It is highly approximate and empirical, but the next level of sophistication is very complex, and sometimes not much more accurate.

$$\Delta C_{Lmax\_flaps} = S_{wf} / S_{ref} \, \Delta C_{Lmax\_flaps} K(sweep)$$

where:

S_{wf} = wing area affected by flaps (including chord extension, but not area buried in fuselage)

S_{ref} = reference wing area

ΔC_{lmax_flaps} = increase in two-dimensional C_{lmax} due to flaps

K = an empirical sweepback correction

The wing area affected by flaps is estimated from a plan view drawing. Typical flaps extend over 65% to 80% of the exposed semi-span, with the outboard sections reserved for ailerons. The resultant flapped area ratios are generally in the range of 55% to 70% of the reference area. (See table at the end of this section.)

ΔC_{lmax_flaps} is determined empirically and is a function of flap type, airfoil thickness, flap angle, flap chord, and sweepback. It may be estimated from the expression:

$$\Delta C_{lmax\_flaps} = K_1 \, K_2 \, \Delta C_{lmax\_ref}$$

ΔC_{lmax_ref} is the two-dimensional increment in C_{lmax} for 25% chord flaps at the 50 deg landing flap

angle and is read from the experimentally-determined curve below at the mean thickness ratio of the wing.

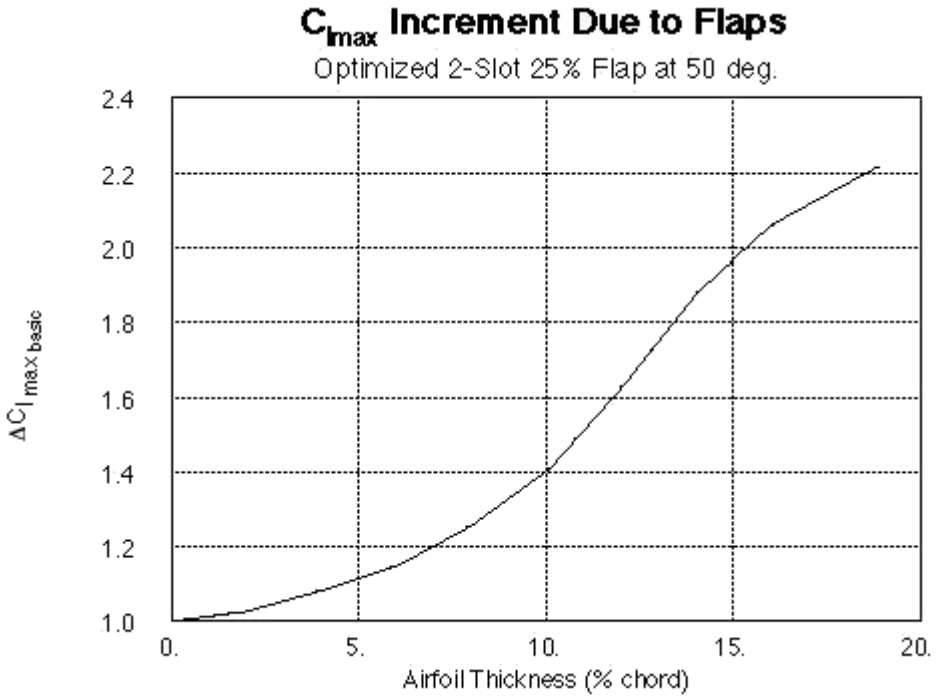

Figure 8. Section C_{lmax} increment due to flaps. The results are for double slotted flaps. For single slotted flap multiply this value by 0.93. For triple slotted flaps, multiply by 1.08.

K_1 is a flap chord correction factor. It includes differences between the flap chord to wing chord ratio of the actual design to that of the reference wing with 25% chord flaps.

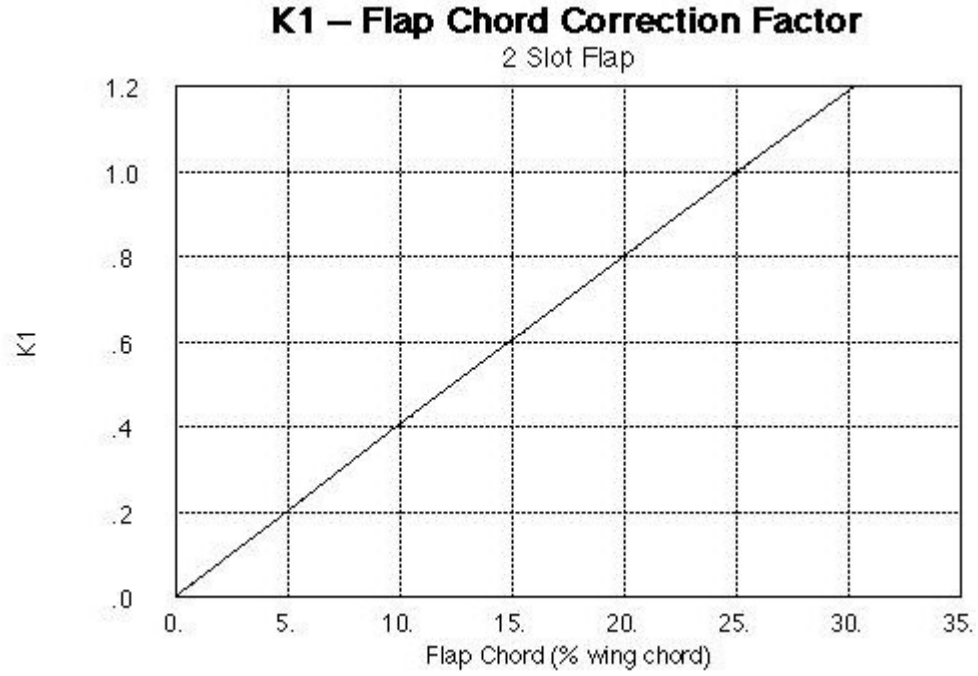

Figure 9. Effect of Flap Chord.

K_2 accounts for the effect of flap angles other than 50 deg.

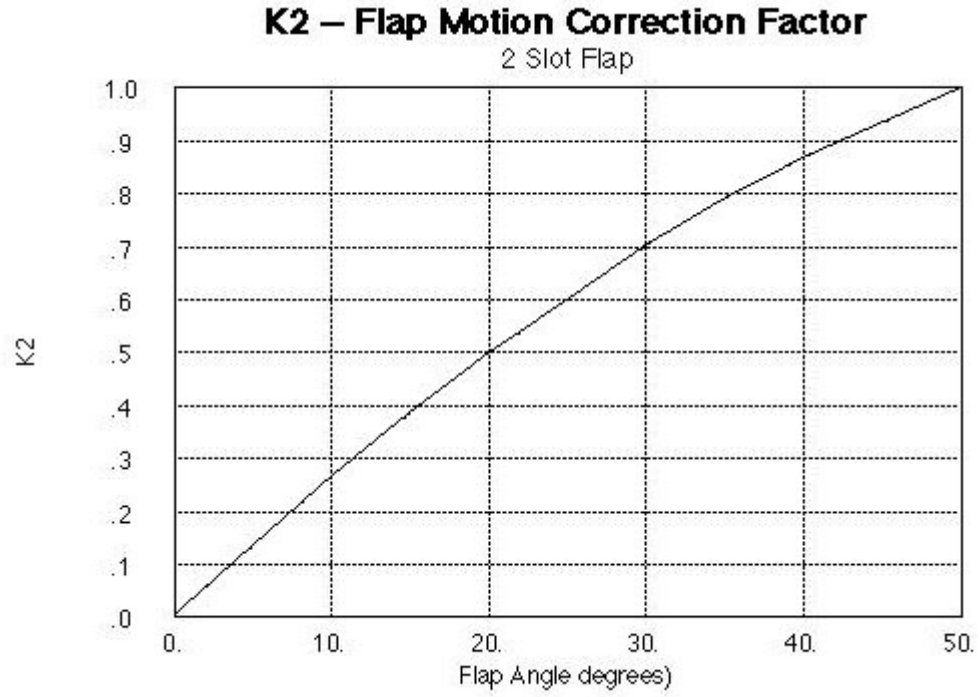

Figure 10. Flap Motion Correction Factor

$K(\Lambda)$ is an empirically-derived sweep-correction factor. It may be estimated from:
$K = (1-0.08*\cos^2(\Lambda)) \cos^{3/4}(\Lambda)$

Effect of Mach Number

The formation of shocks produces significant changes in the airfoil pressure distribution and limits the maximum lift coefficient. In fact, a strong correlation exists between the C_{lmax} of a slat and the C_l at which flow near the slat becomes supersonic. In general, as the freestream Mach number is increased, the aircraft C_{Lmax} is reduced. The figure below shows this effect for the DC-9-30.

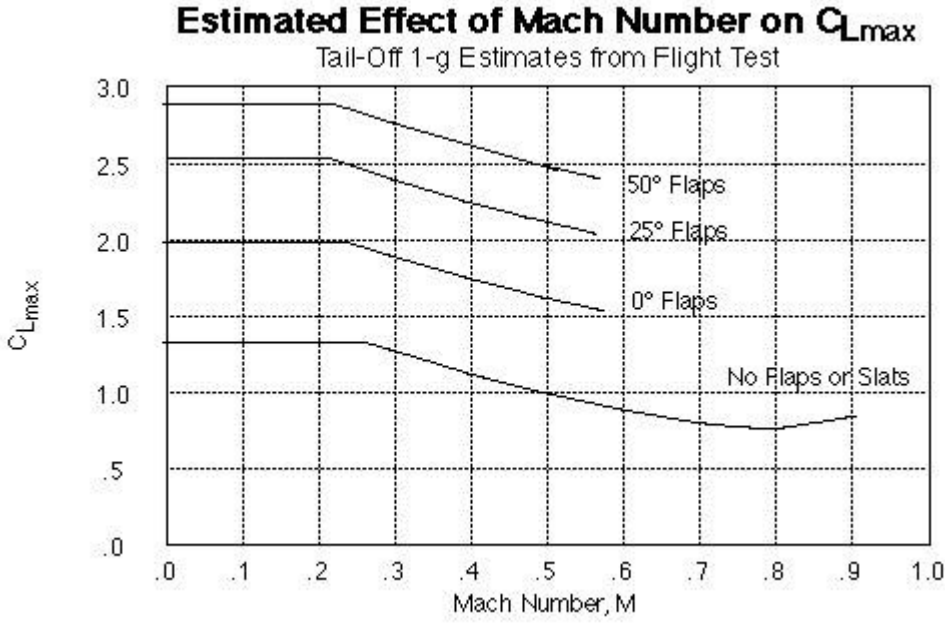

Figure 11. Effect of Mach number on maximum lift.

As a first approximation this data can be used to estimate the effect for another aircraft as follows:

$C_{Lmax}(M) = C_{Lmax\_l.s.} * C_{Lmax\_ref}(M') / C_{Lmax\_l.s.ref}$

Where:

$C_{Lmax\_l.s.}$ is the C_{Lmax} at low speed (Mach number < 0.3)

and M' = Modified Mach number based on equivalent normal Mach = $M*\cos(\Lambda) / \cos(\Lambda_{DC-9})$, where the DC-9, which provides the reference data here, has a sweep of 24.5 deg.

The final figures show the approximate C_{Lmax} values for a number of aircraft.

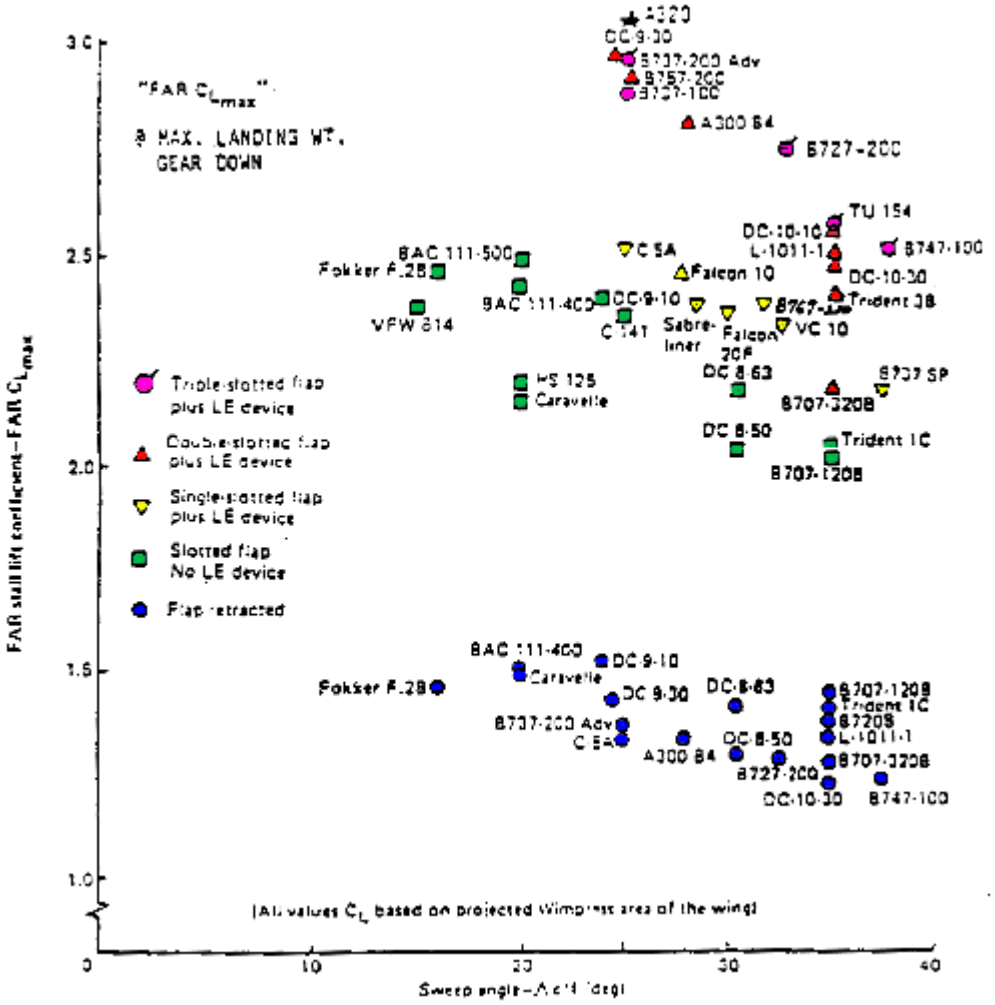

Figure 12. C_{Lmax} Values for a variety of transport aircraft.

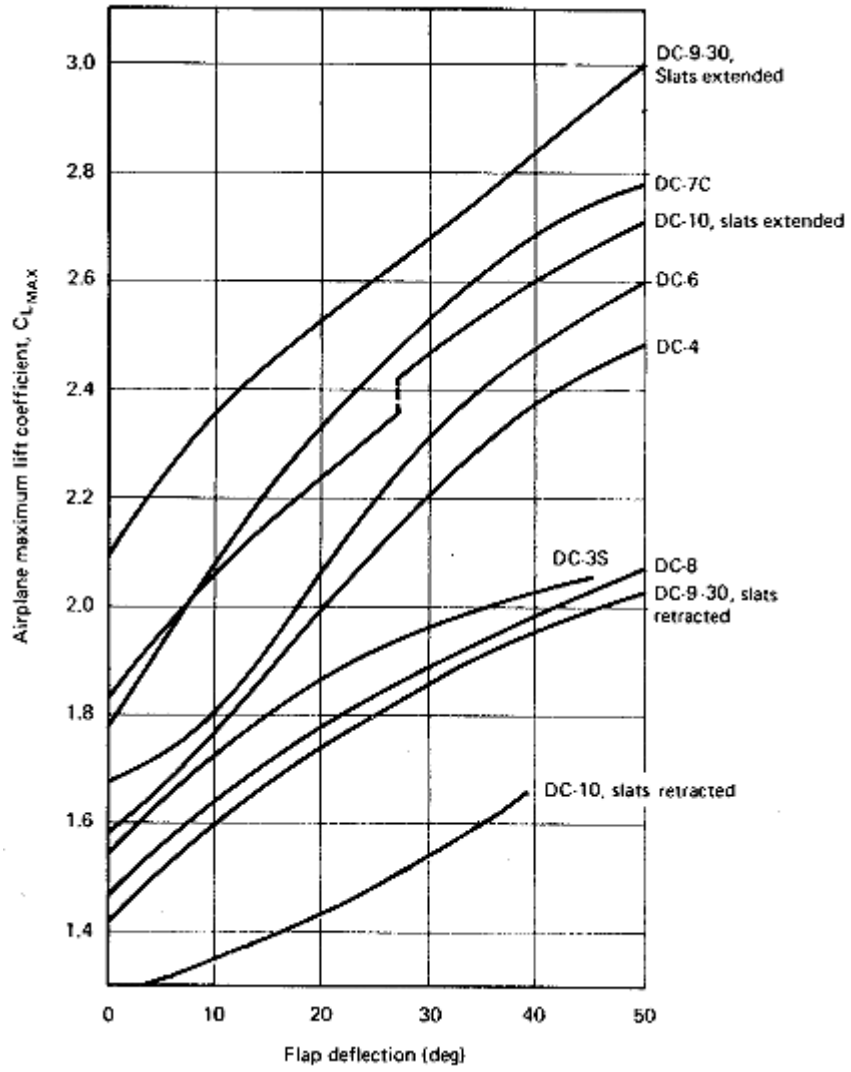

Airplane	S_{wf} / Sref	Flap Type	Flap Chord Ratio	Sweep (deg)
DC-3S	0.575	Split	0.174	10
DC-4	0.560	Single Slot	0.257	0
DC-6	0.589	Double Slot	0.266	0
DC-7C	0.630	Double Slot	0.266	0
DC-8	0.587	Double Slot	0.288	30.5
DC-9-30	0.590	Double Slot	0.360	24.5
DC-10-10	0.542	Double Slot	0.320	35

Figure 13. Effect of Flap and Slat Deflections on C_{Lmax} for several Douglas airplanes. The results are based on the FAA measured stall speeds and reflect the 1 kt/sec deceleration.

Low Aspect Ratio Wings at High Angles of Attack

At high angles of attack, several phenomena usually distinct from the cruise flow appear. Usually part of the wing begins to stall (separation occurs and the lift over that section is reduced). An approximate way to predict when this will occur on well-designed high aspect ratio wings is to look at the C_l distribution over the wing and determine the wing C_L at which some section (the critical section) reaches its 2-D maximum C_l.

When the sweep is very large, or aspect ratio low, this approach does not work. Separation tends to occur near the leading edge of the wing, but unlike in the low sweep situation, the separated region is not large and does not reduce the lift. Instead, the flow rolls up into a vortex that lies just above the wing surface.

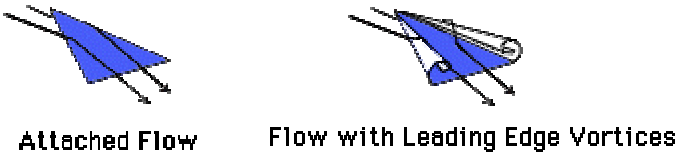

Rather than reducing the lift of the wing, the leading edge vortices, increase the wing lift in a nonlinear manner. The vortex can be viewed as reducing the upper surface pressures by inducing higher velocities on the upper surface.

The net result can be large as seen on the plot here.

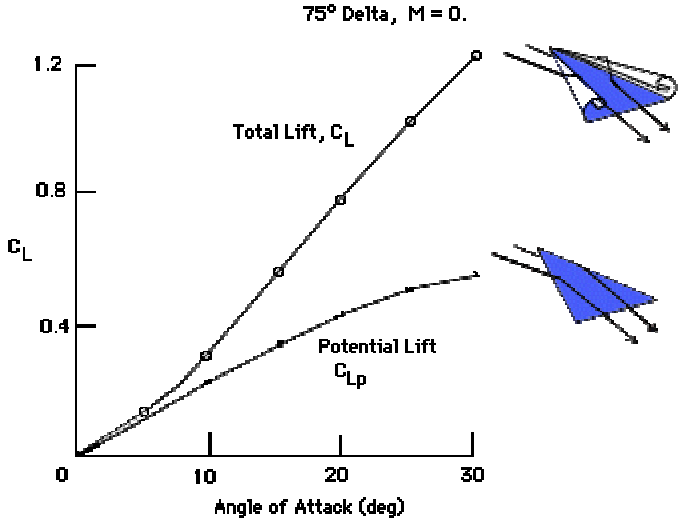

The effect can be predicted quantitatively by computing the motion of the separated vortices using a nonlinear panel code or an Euler or Navier-Stokes solver.

This figure shows computations from an unsteady non-linear panel method. Wakes are shed from leading and trailing edges and allowed to roll-up with the local flow field. Results are quite good for thin wings until the vortices become unstable and "burst" - a phenomenon that is not well predicted by these methods. Even these simple methods are computation-intensive.

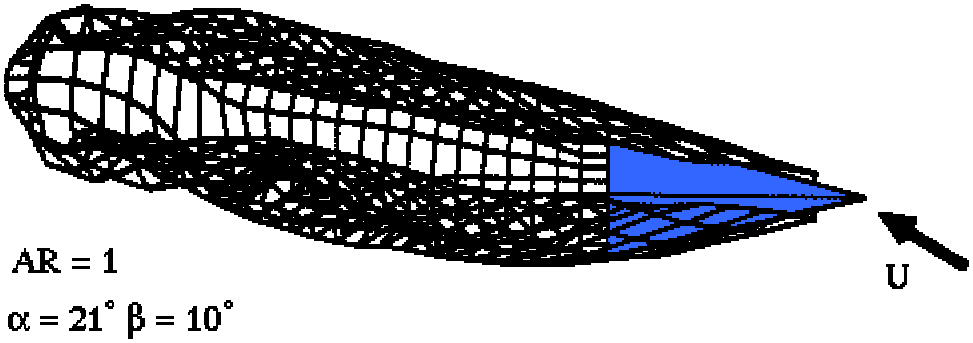

Polhamus Suction Analogy

A simple method of estimating the so-called "vortex lift" was given by Polhamus in 1971. The Polhamus suction analogy states that the extra normal force that is produced by a highly swept wing at high angles of attack is equal to the loss of leading edge suction associated with the separated flow. The figure below shows how, according to this idea, the leading edge suction force present in attached flow (upper figure) is transformed to a lifting force when the flow separates and forms a leading edge vortex (lower figure).

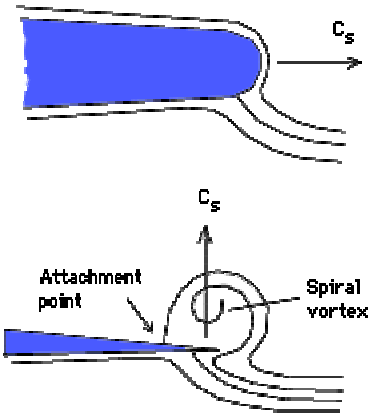

The suction force includes a component of force in the drag direction. This component is the difference between the no-suction drag:
$C_{Di} = C_n \sin a$, and the full-suction drag: $C_L^2 / \pi AR$
where α is the angle of attack.

The total suction force coefficient, C_s, is then:
$C_s = (C_n \sin \alpha - C_L^2/\pi AR) / \cos \Lambda$

where Λ is the leading edge sweep angle. If this acts as an additional normal force then:
$C_n' = C_n + (C_n \sin \alpha - C_L^2/\pi AR) / \cos \Lambda$

and in attached flow:
$C_L = C_{La} \sin \alpha$ with $C_n = C_L \cos \alpha$

Thus, $C_n' = C_L \cos \alpha + (C_L \cos \alpha \sin \alpha - C_L^2/\pi AR) / \cos \Lambda$
$= C_{La} \sin \alpha \cos \alpha + (C_{La} \sin \alpha \cos \alpha \sin \alpha - (C_{La} \sin \alpha)^2/\pi AR) / \cos \Lambda$
$= C_{La} \sin \alpha \cos \alpha + C_{La}/ \cos \Lambda \sin^2 \alpha \cos \alpha - C_{La}^2/(\pi AR \cos \Lambda) \sin^2 \alpha$

$C_L' = C_{La} [\sin \alpha \cos^2 \alpha + \sin^2 \alpha \cos^2 \alpha /\cos \Lambda - C_{La}/(\pi AR \cos \Lambda) \cos \alpha \sin^2 \alpha]$
$= C_{La} \sin \alpha \cos \alpha (\cos \alpha + \sin \alpha \cos \alpha/ \cos \Lambda - C_{La} \sin \alpha /(\pi AR \cos \Lambda))$

If we take the low aspect ratio result: $C_{La} = \pi AR/2$, then:
$C_L ' = \pi AR/2 \sin \alpha \cos \alpha (\cos \alpha + \sin \alpha \cos \alpha/ \cos \Lambda - \sin \alpha /(2 \cos \Lambda))$

Cross-Flow Drag Analogy

An even simpler method of computing the nonlinear lift is to use the cross-flow drag analogy. The idea is to add the drag force that would be associated with the normal component of the freestream velocity and resolve it in the lift direction. The increment in lift is then simply:

$\Delta C_L = C_{Dx} \sin^2\alpha \cos\alpha$.

The plot below shows each of these computations compared with experiment for a 80° delta wing (AR = 0.705). In these calculations a cross-flow drag coefficient of 2.0 was used.

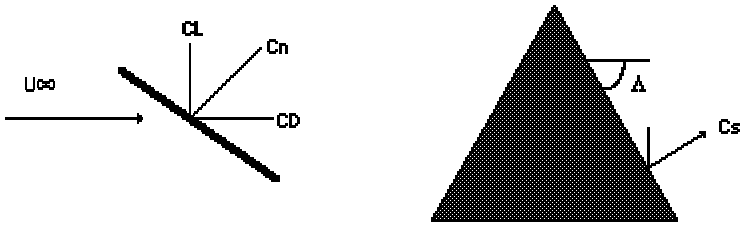

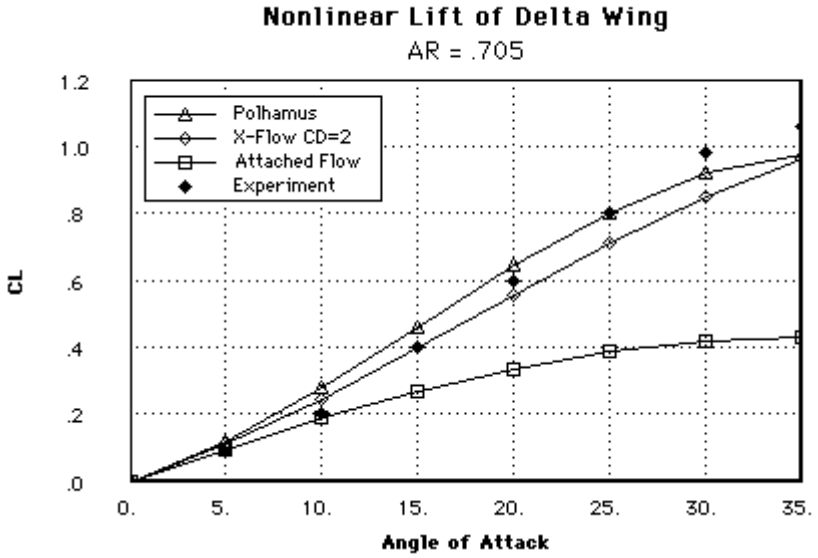

Another case with much higher aspect ratio is shown below. Note that the very simple model seems to do nearly as well as the more involved suction analogy.

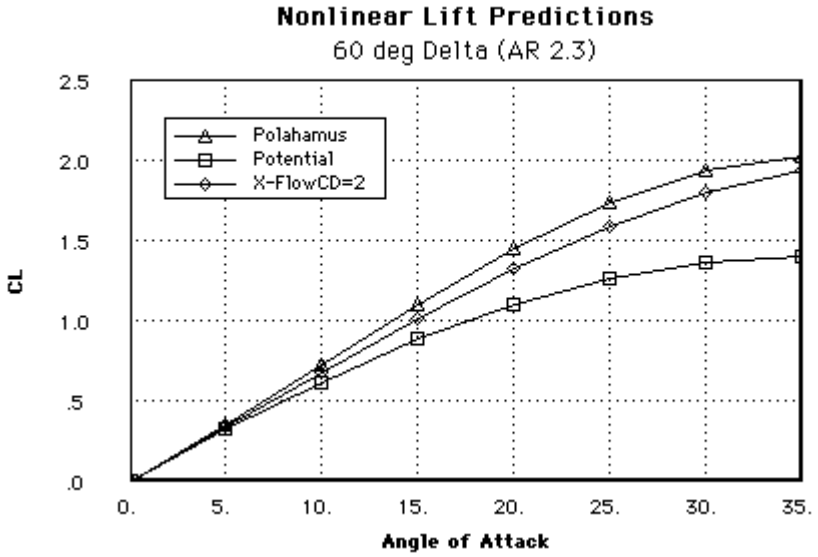

The maximum lift of a low aspect ratio wing is significantly increased by the presence of these vortices and is limited either by vortex bursting or by allowable angle of attack. Vortex bursting is a phenomenon in which the structured character of the vortex is destroyed resulting in a loss of most of the vortex lift. It occurs due to adverse pressure gradients acting on the vortex. When the vortex burst occurs on the wing (as opposed to downstream of the wing) the lift drops substantially. Although there are some empirical methods for predicting vortex burst, the phenomenon is quite complex and difficult to predict accurately. For many SST designs, however, the maximum C_L may be predicted by assuming that the vortex does not burst at the maximum permissible angle of attack. Because of the length of the fuselage, this angle may be restricted to a value of 10-13 degrees. Using this value in the above expression for C_L leads to a reasonable estimate for maximum lift on such designs.

A flow pattern, similar to that of the highly swept delta wing, is found at the tips of low aspect ratio wings and over fuselages. The vortex formation significantly increases the lift in these cases as well. Especially in the case of fuselage vortices, the airplane stability is affected. Interaction with downstream surfaces is often important, but hard to predict. Computations of lift at a specified angle using the cross-flow drag analogy can easily include the component associated with fuselage lift as well.

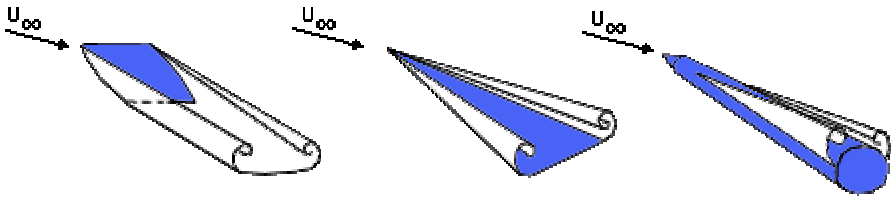

Flaps are often not used on SST designs due to difficulties with longitudinal trim. Designs with tail surfaces or canards can employ some flaps, increasing the effective alpha limit by 2-3 degrees. Clearly, conventional slats do not help these designs as they produce little change in C_L at a given angle of attack. However, studies have shown that some types of leading edge vortex flaps, intended to strengthen the leading edge vortices can be used to further increase the maximum usable C_L.